Analytica Chimica Acta: X 3 (2019) 100030

Contents lists available at ScienceDirect

Analytica Chimica Acta: X

journal homepage: www.journals.elsevier.com/analytica-chimica-acta-x

Red blood cells membrane micropolarity as a novel diagnostic indicator of type 1 and type 2 diabetes

Giada Bianchetti [a, b, 1], Flavio Di Giacinto [a, b, 1], Dario Pitocco [a, c], Alessandro Rizzi [a, c], Gaetano Emanuele Rizzo [a, c], Francesca De Leva [a, c], Andrea Flex [a, d], Enrico di Stasio [a, e], Gabriele Ciasca [a, b], Marco De Spirito [a, b, **], Giuseppe Maulucci [a, b, *]

[a] Fondazione Policlinico Universitario A, Gemelli IRCSS, Rome, Italy
[b] Istituto di Fisica, Università Cattolica Del Sacro Cuore, Rome, Italy
[c] Diabetes Care Unit, Università Cattolica Del Sacro Cuore, Rome, Italy
[d] Cardiovascular Disease Division, Università Cattolica Del Sacro Cuore, Rome, Italy
[e] Istituto di Biochimica Clinica, Università Cattolica Del Sacro Cuore, Rome, Italy

ARTICLE INFO

Article history:
Received 6 September 2019
Received in revised form
9 October 2019
Accepted 10 October 2019
Available online 14 October 2019

Keywords:
Diabetes mellitus
Membrane micropolarity
Red blood cells
Fluorescence lifetime microscopy
Metabolic imaging
Personalized medicine

ABSTRACT

Classification of the category of diabetes is extremely important for clinicians to diagnose and select the correct treatment plan. Glycosylation, oxidation and other post-translational modifications of membrane and transmembrane proteins, as well as impairment in cholesterol homeostasis, can alter lipid density, packing, and interactions of Red blood cells (RBC) plasma membranes in type 1 and type 2 diabetes, thus varying their membrane micropolarity. This can be estimated, at a submicrometric scale, by determining the membrane relative permittivity, which is the factor by which the electric field between the charges is decreased relative to vacuum. Here, we employed a membrane micropolarity sensitive probe to monitor variations in red blood cells of healthy subjects (n=16) and patients affected by type 1 (T1DM, n=10) and type 2 diabetes mellitus (T2DM, n=24) to provide a cost-effective and supplementary indicator for diabetes classification. We find a less polar membrane microenvironment in T2DM patients, and a more polar membrane microenvironment in T1DM patients compared to control healthy patients. The differences in micropolarity are statistically significant among the three groups ($p<0.01$). The role of serum cholesterol pool in determining these differences was investigated, and other factors potentially altering the response of the probe were considered in view of developing a clinical assay based on RBC membrane micropolarity. These preliminary data pave the way for the development of an innovative assay which could become a tool for diagnosis and progression monitoring of type 1 and type 2 diabetes.
© 2019 The Authors. Published by Elsevier B.V. This is an open access article under the CC BY-NC-ND license (http://creativecommons.org/licenses/by-nc-nd/4.0/).

1. Introduction

Diabetes mellitus is a chronic metabolic disease caused by deficiency or diminished effectiveness of endogenous insulin. This pathology is on the rise across the globe: according to the International Diabetes Federation statistics, it was estimated that the number of adults with diabetes in the world had increased from 108 million in 1980 to 422 million in 2014. According to the American Diabetes Association [1], four general categories of diabetes mellitus exist: T1DM (due to β-cell destruction, usually leading to absolute insulin deficiency); T2DM (due to a progressive insulin secretory defect on the background of insulin resistance); Gestational diabetes mellitus (diabetes diagnosed in the second or third trimester of pregnancy that is not clearly overt diabetes); other specific types of diabetes (due to other causes, e.g., monogenic diabetes syndromes, diseases of the exocrine pancreas, and drug- or chemical-induced diabetes). Among these four types, T1DM and T2DM represent the most numerous categories (more than 97% of the diagnoses). Clinically, the category is usually

Abbreviations: DMPC, dimyristoylphosphatidylcholine; DPPC, dipalmitoilphosphatidylcholine; HbA1c, glycated Haemoglobin; HDL, high-density lipoproteins; HDL-C, high-density lipoprotein cholesterol; LDL, low-density lipoproteins; LDL-C, low-density lipoprotein cholesterol; PC, phosphatydilcholine; RBC, red blood cells; T1DM, Type 1 Diabetes Mellitus; T2DM, Type 2 diabetes Mellitus.

* Corresponding author. Largo Francesco Vito, 1, 00168, Rome, Italy.
** Corresponding author. Largo Francesco Vito, 1, 00168, Rome, Italy.
E-mail addresses: marco.despirito@unicatt.it (M. De Spirito), giuseppe.maulucci@unicatt.it (G. Maulucci).
[1] These authors contributed equally to this work.

https://doi.org/10.1016/j.acax.2019.100030
2590-1346/© 2019 The Authors. Published by Elsevier B.V. This is an open access article under the CC BY-NC-ND license (http://creativecommons.org/licenses/by-nc-nd/4.0/).

determined by tests, such as fasting plasma insulin, insulin releasing test, C-Peptide test, insulin autoantibodies and islet cell autoantibodies. Some of these tests are subject to age effects or are incomplete to diagnose diabetes, and, due to the rising number of patients needing a diagnosis, a cost-effective and supplementary indicator for diabetes classification is needed.

In this paper, we propose the determination of red blood cell membrane micropolarity as a diagnostic indicator of diabetes type. Membrane micropolarity can be estimated, at a submicrometric scale, by fluorescent probes able to determine the membrane relative permittivity, which is the factor by which the electric field between the charges is decreased relative to vacuum. Membrane micropolarity depends both on membrane composition and membrane phase state, which modulates the interaction between water molecules and membranes giving rise to different structures of interfacial water from the bulk [2]. Micropolarity can thus be a superior tool with respect to traditional and expensive lipidomic tools, because, in addition to composition, integrates also the information of the physical phase state in its outcome (i.e. liquid-ordered, liquid-disordered, solid-ordered). Among the factors modulating membrane micropolarity, glycosylation, oxidation and other post-translational modifications of membrane and transmembrane proteins, as well as impairment in cholesterol homeostasis, can alter lipid density, packing and interactions of Red blood cells (RBC) plasma membranes. Cholesterol has a huge impact on membrane structure and phase state because it is found in high concentrations in animal cell membranes, typical concentrations being around 20–30 mol% and ranging up to 50 mol% in RBC [3]. Moreover, it is a donor and acceptor of hydrogen bonds, thus affecting the interactions of lipid headgroups with water at the bilayer interface [4–6]. In cells that cannot synthesize lipids on their own, as RBC, cholesterol exchange with plasma lipoproteins is, therefore, one of the main determinants of micropolarity change [7].

The rationale at the basis of the selection of membrane RBC micropolarity as a diagnostic indicator for the type of diabetes relies on the fact that the systemic environmental parameters that alter glycosylation of proteins, oxidation of proteins and membranes, as well as the dynamic flux of cholesterol between membranes and lipoproteins are different in healthy, T1DM and T2DM subjects [8,9], and are naturally sensed by the physical state of the RBC water layer membrane [10].

We have already provided evidence that RBC membrane micropolarity is significantly altered in T1DM and can be an ideal biomarker for monitoring the development of T1DM complications [10]. In this article, we retrieve membrane micropolarity maps at submicrometric scale of erythrocytes of healthy subjects and patients affected by T1DM and T2DM by using the solvatochromic and lipophilic probe Laurdan, characterized by a solvent-dependent emission spectrum [11,12]. In membranes, Laurdan is fluorescent with at least two excited states: the locally excited state, which is intrinsic to the fluorophore, and an internal charge transfer state created by a larger dipole moment. The latter causes the reorientation of the surrounding water molecules to align with the Laurdan dipole moment. This process consumes the energy of excited Laurdan molecules so that the frequency of the emitted photons is decreased, which causes a redshift in the emission wavelength. This process, referred to as solvent relaxationhttps://www.sciencedirect.com/science/article/pii/S0006349518310191?via%3Dihub - bib19, allows a direct measurement of membrane micropolarity [13]. Depending on the number of the surrounding water molecules, Laurdan displays a varying degree of solvent relaxation that can be used to describe the lipid environment in membranes. RBC membrane micropolarity is quantified with submicrometric resolution by an index called GP, going from −1 (highest membrane micropolarity) to +1 (lowest membrane micropolarity) [14]. This index allows distinguishing the effects of the steady-state flux of phospholipids and cholesterol in these patients and the environmentally-driven spatial phase reorganizations. Among the several factors causing membrane micropolarity variations, the role of the cholesterol pool in determining these variations is deeply investigated. This study, relying on the fact that worldwide from 90 to 95% of diagnosed cases of diabetes are type 2 diabetes, constitutes a significant broadening of the scope of this innovative assay which could become a tool for diagnosis and progression monitoring not only of type one but also of type 2 diabetes.

2. Methods

2.1. Sample preparation and selection and determination of plasma lipoprotein distribution

Samples of human RBC are prepared as reported previously [10], seeded on a multi-well plate and directly visualized on the microscope. The determination of blood analytes was performed by ADVIA-Chemistry Cholesterol_2, ADVIA-Chemistry D-HDL and ADVIA-Chemistry Triglycerides_2 tests on Siemens ADVIa Chemistry XPT instrument. LDL concentration were estimated according to Friedwald formula: LDL = Total cholesterol − (HDL cholesterol + Triglycerides/5). To assess the effects of blood lipoprotein compositions 50 subjects are enrolled: 16 healthy control (CTRL), 10 subjects with T1DM and 24 subjects with T2DM. For CTRL group inclusion criteria are the absence of evidence of any active or chronic disease following a detailed medical and surgical history, a Body Mass Index (BMI) of 18–30 kg/m^2 inclusive, with bodyweight in the range of 50–100 kg, absence of abnormal values following a complete physical examination including vital signs, 12-lead ECG, hematology, blood chemistry, serology and urinalysis. For T1DM group inclusion criteria are the diagnosis of T1DM, age ≥18 years old. For T2DM group inclusion criteria were the diagnosis of T2DM. For T2DM group exclusion criteria were the diagnosis of T1DM, of Maturity-Onset Diabetes of the Young (MODY), of latent autoimmune diabetes of adults (LADA). For all groups, exclusion criteria are previous pancreatic surgery or chronic pancreatitis, medical history of cancer in the last five years prior to the enrollment, presence of any blood dyscrasia causing hemolysis or unstable RBC.

T1DM and T2DM patients are under treatment: T1DM patients are treated with multiple daily injections of insulin or continuous subcutaneous administration through an insulin pump. T2DM patients are treated with metformin in combination with lifestyle modifications. Patients who did not achieve the HbA1C target less than 7% and do not have atherosclerotic cardiovascular disease or chronic kidney disease, are related with a combination of metformin and glucose-lowering drugs (sulfonylurea, thiazolidinedione, dipeptidyl peptidase 4 (DPP-4) inhibitor, SGLT2 inhibitor, GLP-1 receptor agonist), or basal insulin; the choice of which agent to add is based on drug-specific effects and patient factors.

For patients of all ages with diabetes and atherosclerotic cardiovascular disease or 10- year atherosclerotic cardiovascular disease risk >20%, high-intensity statin therapy is added to lifestyle therapy, to obtain approximately a 50% reduction in low-density lipoproteins (LDL) cholesterol. For patients who do not tolerate the intended intensity of statin, the maximally tolerated statin dose is used.

All research involving human participants have been approved by the ethical committee of Università Cattolica del Sacro Cuore, Rome, Italy, and all clinical investigation have been conducted according to the principles expressed in the Declaration of Helsinki.

All patients have provided informed consent for study participation.

2.2. Membrane micropolarity measurements on RBC

The fluorescence spectrum of the probe Laurdan, which incorporates into the lipid phase in the membrane, is correlated to its physical state. Laurdan's excited-state relaxation, independent of the head-group type in phospholipids, is highly sensitive to the presence and mobility of water molecules within the membrane bilayer, yielding information on membrane micropolarity by a shift in its emission spectrum depending on the surrounding lipid phase state (i.e. bluish in ordered, gel phases and greenish in disordered, liquid-crystalline phases) [16]. Two-photon infrared excitation techniques have been successfully applied to detect Laurdan emission [14,17]. By using this probe, coexisting lipid domains are characterized based on their distinctive fluorescence spectra and dual-wavelength ratio measurements, which map changes in the structure of PM. Cells are imaged with a Nikon A1-MP confocal microscope (within 1 h from extraction). 1 μl of Laurdan 1 mM stock solution (Molecular Probes, Inc., Eugene, OR, USA) is added per milliliter of Dulbecco's Modified Eagle's Medium (DMEM). For the determination of GP, cells are acquired with a Nikon A1-MP confocal microscope equipped with a 2-photon Ti:Sapphire laser (Mai Tai, Spectra Physics, Newport Beach, CA) producing 80-fs pulses at a repetition rate of 80 MHz. Laurdan intensity images are recorded simultaneously with emissions in the ranges of 425–475 nm and 500–550 nm and imaging was performed at 37 °C. All images are acquired at 200 nm pixel resolution (60× objective). Background values are measured and subtracted for each image, and cells different from RBC, debris or other aggregates are removed to avoid biases in the analysis. As a normalized ratio of the intensity at the two emission wavelength regions, the generalized polarization (GP) provides a measure of membrane order(-high membrane micropolarity, low GP) to green (low membrane micropolarity, high GP). The GP index (1) is calculated for each pixel using the two Laurdan intensity images $I_{425\text{-}475}$ and $I_{500\text{-}550}$ by using the program "Ratiometric Image processor"[21]. According to the $GP = (I_{425\text{-}475} - G\, I_{500\text{-}550})/(I_{425\text{-}475} + G\, I_{500\text{-}550})$, G is a calibration factor obtained by measuring laurdan fluorescence in DMSO as in Ref. [17]. GP index is independent of excitation intensities, probe concentrations, and other artifacts, relying on the ratiometric properties of the probe [18,19].

2.3. Spectral phasors

Spectral phasor analysis is an analytical method for the analysis of spectral fluorescence images and lifetime images [20,21]. We use spectral images acquired at 780 nm excitation with a PML-SPEC 16 GaAsP 16 channel spectral detector (bandwidth 12.5 nm, wavelength range 408 nm–608nm). Excitation at 780 nm induced negligible autofluorescence, since two-photon excitation of intracellular metabolites is centered at 740 nm. Each pixel in the spectral image contains the emission spectrum at that pixel. Therefore, an emission curve is associated with every pixel. The spectral phasor transformation calculates the normalized Fourier transform of a given spectrum. For each Fourier harmonic, two coordinates are calculated: *g* corresponds to the real part of the Fourier transform and *s* corresponds to the imaginary part of the transform. The equations [19] needed to obtain these values are reported below:

$$g_{ij} = \frac{\int_{\lambda_{min}}^{\lambda_{max}} I_{ij}(\lambda)\cos\left(\frac{2\pi(\lambda-\lambda_{min})}{\lambda_{max}-\lambda_{min}}\right)d\lambda}{\int_{\lambda_{min}}^{\lambda_{max}} I_{ij}(\lambda)d\lambda} \xrightarrow{discrete\ signal} g_{ij} = \frac{n\sum_{k=1}^{n} I_{ijk}\left(\sin\left(\frac{2\pi k}{n}\right) - \sin\left(\frac{2\pi(k-1)}{n}\right)\right)}{2\pi\sum_{k=1}^{n} I_{ijk}} \quad (1)$$

$$s_{ij} = \frac{\int_{\lambda_{min}}^{\lambda_{max}} I_{ij}(\lambda)\sin\left(\frac{2\pi(\lambda-\lambda_{min})}{\lambda_{max}-\lambda_{min}}\right)d\lambda}{\int_{\lambda_{min}}^{\lambda_{max}} I_{ij}(\lambda)d\lambda} \xrightarrow{discrete\ signal} s_{ij} = \frac{n\sum_{k=1}^{n} I_{ijk}\left(\cos\left(\frac{2\pi(k-1)}{n}\right) - \cos\left(\frac{2\pi k}{n}\right)\right)}{2\pi\sum_{k=1}^{n} I_{ijk}} \quad (2)$$

λ in Eqs. (1) and (2) is the emission wavelength, λmin and λmax indicate the acquisition range, k is the number which identifies the spectral channel and Iijk is the signal relative to the pixel ij and the k-th channel. These two numbers, g and s, are used as coordinates in a scatter plot, the phasor plot. Coincident spectra are projected on the same point, while different spectra are projected on different points. When an image contains several different spectra, the relative phasor plot contains a cloud of points scattered throughout the plane. Selected regions in the phasor plot can be remapped to the original fluorescence image, thus providing segmentation based on pixels with similar spectral properties. All the spectral phasors and the images are analyzed with the freeware software PhasorM [22].

2.4. Fluorescence lifetime microscopy of laurdan emission

FLIM data for RBC are acquired with a Nikon A1-MP confocal microscope equipped with a 2-photon Ti:Sapphire laser (Mai Tai, Spectra Physics, Newport Beach, CA) producing 80-fs pulses at a repetition rate of 80 MHz. A PML-SPEC 16 GaAsP (B&H, Germany) multi-wavelength detector coupled to a SPC-830 TCSPC/FLIM device (B&H, Germany) is used to collect the decay data. A 60 × oil-immersion objective, 1.2 NA, is used for all experiments. Laurdan fluorophore is excited at 780 nm. Signals are integrated into the wavelength region 420–460 nm for the blue channel and 500–560 nm for the green channel. For image acquisition, the pixel frame size is set to 512 × 512 and the pixel dwell time was 60μs. The average laser power at the sample is maintained at the mW level. FLIM acquisitions provide for decay curves, *Iij*(t), for each pixel. These are processed by the PhasorM software [22] for the phasor analysis, exactly as was explained for spectral data and they are collected and plotted on the so-called phasor plot. The Equations (3) and (4) used to calculate the g and s coordinates for the lifetime phasor plot are like the one shown for the spectral data but in this case, the summation is done on the time channels:

$$g_{ij} = \frac{\int_{0}^{T} I_{ij}(t)\cos\left(\frac{2\pi t}{T}\right)dt}{\int_{0}^{T} I_{ij}(t)dt} \xrightarrow{discrete\ signal} g_{ij} = \frac{n\sum_{k=1}^{n} I_{ijk}\left(\sin\left(\frac{2\pi k}{n}\right) - \sin\left(\frac{2\pi(k-1)}{n}\right)\right)}{2\pi\sum_{k=1}^{n} I_{ijk}} \quad (3)$$

$$s_{ij} = \frac{\int_0^T I_{ij}(t)\sin\left(\frac{2\pi t}{T}\right)dt}{\int_0^T I_{ij}(t)dt} \xrightarrow{\text{discrete signal}} s_{ij} = \frac{n\sum_{k=1}^{n} I_{ijk}\left(\cos\left(\frac{2\pi(k-1)}{n}\right) - \cos\left(\frac{2\pi k}{n}\right)\right)}{2\pi\sum_{k=1}^{n} I_{ijk}} \quad (4)$$

Parameters in equations (3) and (4) are the same used for equations (1) and (2), replacing the wavelength with the time t and considering T as the total period of acquisition which is considered for the analysis (in our experiments T is equal to 9,8 ns).

2.5. Statistics

Statistical T-tests for sets of biological/biophysical data are performed by R Studio (https://www.rstudio.com/). Baseline characteristics among groups have been compared with ANOVA for parametric variables. Data normality was checked graphically by quartile-quartile plots. A Comparison between groups couple has been made with Tukey's Test.

3. Results

3.1. Effect of cholesterol removal on RBC membrane micropolarity: spectral analysis

To investigate the effect of cholesterol in modulating membrane micropolarity, we perform cholesterol removal experiments on RBC of healthy subjects. In Fig. 1A membrane micropolarity maps of healthy RBC (CTRL) are reported. Each pixel is colored according to its GP values, in a two-colored scale spanning from red (high membrane micropolarity, low GP) to green (low membrane micropolarity, high GP). Since RBC lack interior organelles, laurdan labels just the plasma membrane (PM), and the measured outcome corresponds directly to PM micropolarity. Acute cholesterol depletion by methyl-β-cyclodextrin (MβCD, 10 mM, 3h) induces a PM micropolarity increase (GP decrease), as quantified in the histogram of GP values reported along with the images (Fig. 1A). Average GP shifts from 0.56 ± 0.01 to 0.49 ± 0.02 (Fig. 1B, n=100 RBC per sample, average of n=5 patients). The membrane micropolarity map shows in both cases an anisotropic distribution. It is possible to observe in the images a reduction in the size of high GP domains (low polarity) when cholesterol is depleted.

To get further information about the phase state of the membrane, we perform a spectral analysis of laurdan emission. In Fig. 2A a representative spectrum of laurdan in healthy RBC is reported. The already observed increase in membrane micropolarity induced by MβCD (GP decrease), is quantified by the detectable shift in the emission wavelength towards the green. The spectral analysis provides more information than the dualchannel analysis. In a two-channel analysis, several emission spectra can produce the same outputs (metamers). A multispectral analysis enables the possibility to resolve these coincident emission profiles providing a more comprehensive classification of micropolarity domains. The pixel-resolved Laurdan fluorescence emission spectra can be analyzed by the spectral phasor analysis method [19,23,24]. The spectral phasor transformation assigns, through an algorithm, two numbers at each spectrum in a unique way. These numbers, called g and s, are used as coordinates in a scatter plot, called the phasor plot (Fig. 2A and section 2.3). Clockwise rotation on the phasor plot indicates a shift towards lower wavelengths (high polarity), and vice-versa. Selected regions in the phasor plot can be remapped to the original fluorescence image, thus providing a micropolarity driven segmentation: pixels characterized by a similar micropolarity value can be grouped and shown on the image with a characteristic color scale. In Fig. 2A, pixels selected in the blue region of interest (ROI) corresponds to the regions with the highest membrane micropolarity, while the pixels in the red ROI corresponds to the lowest membrane micropolarity. Regions characterized by an intermediate micropolarity value are shown in a pseudo-colored scale from red to blue (figure look-up table along with the phasor plot in Fig. 2A). The color-coded regions of interest are chosen as rectangles, with the shortest sides perpendicular to the

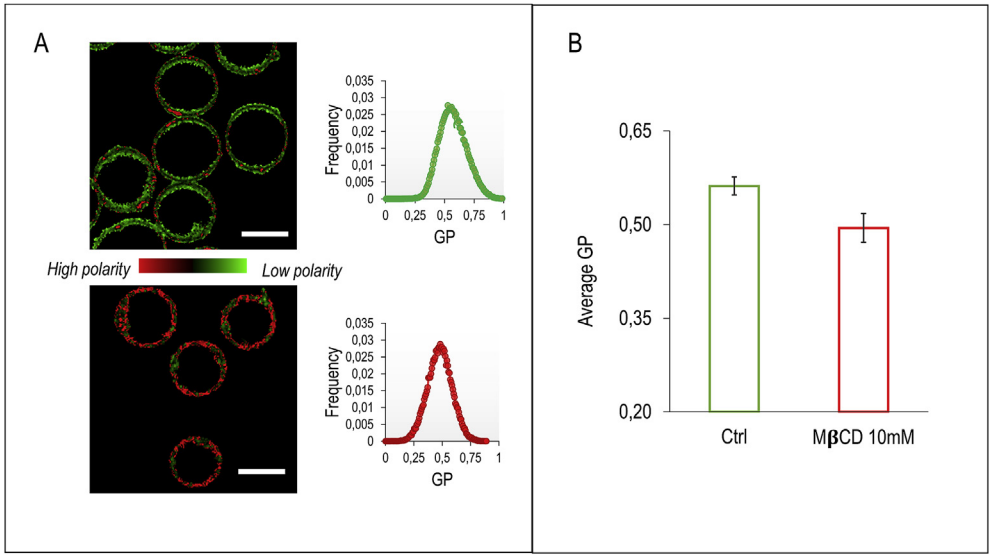

Fig. 1. *Micropolarity maps of control and cholesterol-depleted RBC.* (A) A representative submicrometric membrane micropolarity map of RBC. According to the GP values, each pixel's color spans from red (high membrane micropolarity, low GP) to green (low membrane micropolarity, high GP). Treatment with 10 mM methyl-β-cyclodextrin, by depleting cholesterol, induces an increase in membrane micropolarity, resulting in a shift of GP distribution towards lower values (scale bar is 10 μm and 7 μm, respectively). (B) Average GP of healthy (green) and MβCD-treated (red) RBC is reported in the histogram. Mean value shifts from 0.56 to 0.49 when cholesterol is removed. Error bars indicate standard deviation of the data. (For interpretation of the references to color in this figure legend, the reader is referred to the Web version of this article.)

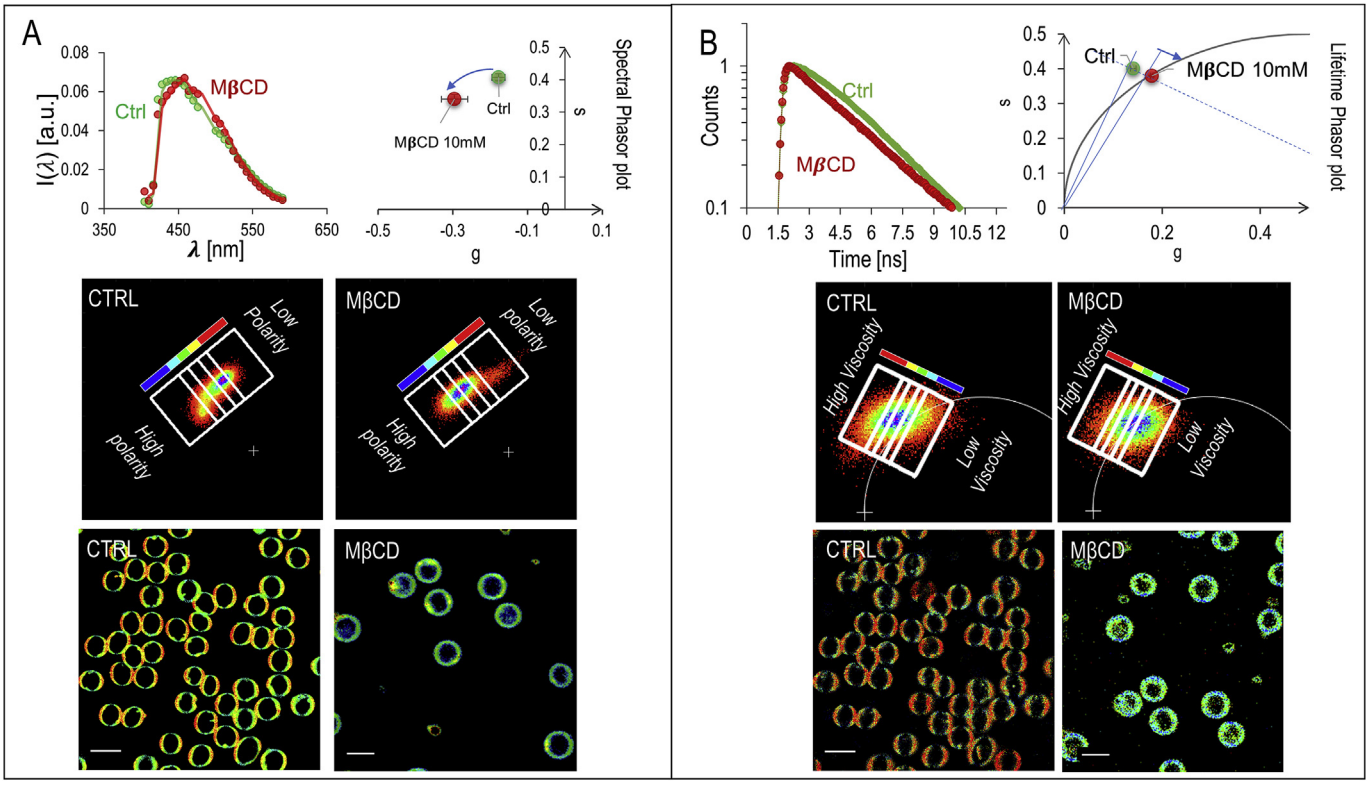

Fig. 2. Spectral and lifetime analysis of laurdan emission of control and cholesterol-depleted RBC (A) Spectral analysis of laurdan's fluorescence. The normalized emission spectrum of the probe in healthy RBC is reported for control (green) and MβCD-treated (red) RBC, respectively. The red-shift in the emission wavelength as a consequence of the increased membrane micropolarity, results in a clockwise rotation of the center of mass of the clouds on the phasor plot. The spectral phasor analysis allows a fine polarity driven segmentation for RBC membranes. Pixels selected in the blue ROI corresponds to the regions with the highest membrane micropolarity, while the pixels in the red ROI corresponds to the lowest membrane micropolarity. Regions characterized by an intermediate micropolarity value are shown in a pseudo-colored scale from red to blue. Figure lookup table is reported along with the phasor plot. (B) decay curves in the green channel (emission 540/50 nm) of control and cholesterol depleted RBC. Decay curves are analyzed through lifetime phasor transformation to quantify and visualize changes in viscosity. The phasor distributions integrated for N = 100 cells (in each category) show the center of mass of the phasor that lies outside of the universal circle for the control cells, indicating a non-exponential decay. Upon depletion of cholesterol, the point rotates towards the universal circle. The lifetime phasor analysis allows a viscosity driven segmentation, from blue (low viscosity) to red (high viscosity). Figure lookup table is reported along with the phasor plot. The color-coded regions of interest are chosen as rectangles, with the shortest sides perpendicular to the line connecting the center of mass of the clouds in the phasor plot of untreated and treated cells. (For interpretation of the references to color in this figure legend, the reader is referred to the Web version of this article.)

line connecting the center of mass of the clouds in the phasor plot of untreated and treated cells. In RBC the low-polarity regions are organized in sub-micrometric domains characterized by a high-packing density. When cells are treated with MβCD, a concomitant decrease of polarity and the packing degree of membranes is observed.

3.2. Effect of cholesterol removal on RBC membrane micropolarity: lifetime analysis

In membranes, the solvent relaxation (decrease in GP-increase in micropolarity), analyzed so far, depends on the number of the surrounding water molecules, and thus increases with membrane hydration levels [25,26]. This effect can be also revealed by a decrease of the fluorescence lifetime due to the enhanced emission from the relaxed state, which is characterized by a lower lifetime. Another quantity that can be measured analyzing the fluorescence decay is the rate of solvent relaxation, obtained from measuring the rate of the spectral shift [27,28]. The speed of solvent relaxation is related to the rotational mobility of the water molecules within the membrane and is referred to as membrane microviscosity [25]. When the rate of spectral relaxation is in the picosecond scale, the temporal resolution of the time-correlated single photon counting devices is not able to resolve any changes. However, in very viscous environments the time scale of relaxation can increase up to the nanosecond time scale. In this context, the change in membrane polarity due to water hydration from the effects due to viscosity can be uncovered by analyzing the decay time in the green channel (emission 540/50 nm) [27,28]. The excited-state decay in the green channel presents two apparent decays: one is due to the decay of the standard fluorescence emission from the relaxed state, and the other is an apparent decay time due to the populating process from the locally excited state to the relaxed state. The two processes give rise to a visible non-exponential decay in control cells (Fig. 2B), in which cholesterol is physiologically present, which becomes again exponential in the cholesterol-depleted cells. In the latter, we find a decrease of the apparent lifetimes of the green channel indicating a less viscous environment and a decrease of the lifetime of the relaxed state reflecting a more polar environment. To dissect these two contributions we can use the lifetime phasor transformation to quantify and visualize changes in viscosity. The phasor lifetime approach is ideal in this case since changes in decay times can be quantified without the requirement of an explicit mathematical model. In a way analogous to the spectral phasor transformation, to each lifetime decay curve are uniquely assigned two numbers. These numbers, called *g* and *s*, are used as coordinates in a lifetime phasor plot (2B and section 2.4). If the exponential is a single decay, the point lies on the universal semi-circle (solid line Fig. 2B). If the exponential is composed of multiple decays, it lies inside the exponential circle. If the decay does not fall in the latter categories,

thus being non-exponential, it falls outside of the universal circle [21]. The phasor distribution integrated for control cells (n=100) is shown for the green channel. The center of mass of the phasor lies outside of the universal circle for the control cells, indicating a non-exponential decay. Upon depletion of cholesterol, the point rotates towards the universal circle. We can thus conclude that in cholesterol-depleted cells the environment is less viscous. As we did in the spectral phasor approach, we can select regions in the phasor plot and remap them to the original fluorescence images, thus providing a viscosity driven segmentation: pixels characterized by a similar viscosity value can be grouped and shown on the image with a characteristic color scale. The color-coded ROI are chosen as rectangles, with the shortest sides perpendicular to the line connecting the center of mass of the clouds in the phasor plot of untreated and treated cells. From the lifetime images, it is possible to observe that low polarity domains display also higher viscosity.

3.3. *Membrane micropolarity of RBC from healthy subjects and T1DM and T2DM patients*

Next, we investigated if RBC extracted from healthy, T1DM and T2DM patients are characterized by different values of micropolarity. Baseline characteristics among groups have been compared with ANOVA for parametric variables (Table 1). Subjects are comparable for creatinine and low-density lipoprotein cholesterol (LDL-C) values. Subjects with diabetes are comparable for glycated hemoglobin (Table 1). Submicrometric phase state map of healthy, T1DM and T2DM RBC are reported (Fig. 3A). Each pixel is colored, according to its GP values, in a scale spanning from red (high polarity, low GP) to green (low polarity high GP). It is possible to observe from the images that there is a decrease in GP going from T2DM patients, through control, to T1DM patients, reflecting the decrease in the extent of low micropolarity domains regions. In Fig. 3B the box plot shows significant differences among the GP values of the three populations under observation (p values reported in the box plot). To explore the potential effects of selected covariates, intra-Group correlation plots were realized between GP values and Age, Sex, body mass index(BMI), Glycated Haemoglobin (HbA1C), lipid values. From this analysis, a significant ($p<0.05$) effect of the covariates was excluded for the samples under analysis (Fig. S1), thus additional adjustments are not performed. The double box plot of Fig. 3B shows GP average values in each group decreasing with increasing high-density lipoprotein cholesterol (HDL-C) average values, suggesting that the GP value is related to RBC cholesterol content.

Table 1
Characteristics of the 50 participants. Baseline characteristics among groups have been compared with ANOVA for parametric variables. Subjects were comparable for creatinine and LDL-C values. Subjects with diabetes were comparable for glycated hemoglobin(* stands for p<0.05; **p<0.01; ***p<0.001).

Variable	CTRL n=16	T1DM n=10	T2DM n=24	Fisher	Tukey CTRL-T1DM	Tukey CTRL-T2DM	Tukey T1DM-T2DM
Age (years)	44 ± 10	42 ± 10	66 ± 10	1.40 10^{-9}	0.83	1 10^{-7} (***)	2 10^{-7}(***)
BMI (kg/m^2)	23.1 ± 2.4	21.6 ± 3.3	26.9 ± 3.2	4.73 10^{-4}	0.57	0.022(*)	5 10^{-4}(***)
HbA1C (mmol/mol)	36 ± 5	53 ± 8	59 ± 15	3.98 10^{-7}	0.0014(**)	2 10^{-6}(***)	0.325
Total cholesterol (mg/dl)	180 ± 48	189 ± 33	146 ± 42	0.0123	0.87	0.049(*)	0.03(*)
HDL-C (mg/dl)	56 ± 9	74 ± 15	42 ± 12	1.23 10^{-7}	0.0016(**)	0.007(**)	1 10^{-7}(***)
LDL-C (mg/dl)	107 ± 43	101 ± 25	87 ± 30	0.21	0.91	0.2	0.51
Tryglicerides (mg/dl)	78 ± 33	67 ± 53	131 ± 61	2.35 10^{-3}	0.87	0.013(*)	0.008(**)
Creatinine (mg/dl)	0.87 ± 0.12	0.66 ± 0.10	1.12 ± 0.51	0.09	0.91	0.19	0.12
GP	0.601 ± 0.017	0.558 ± 0.019	0.636 ± 0.039	4.62E-08	0.002(**)	0.002(**)	>1 10^{-7}(***)

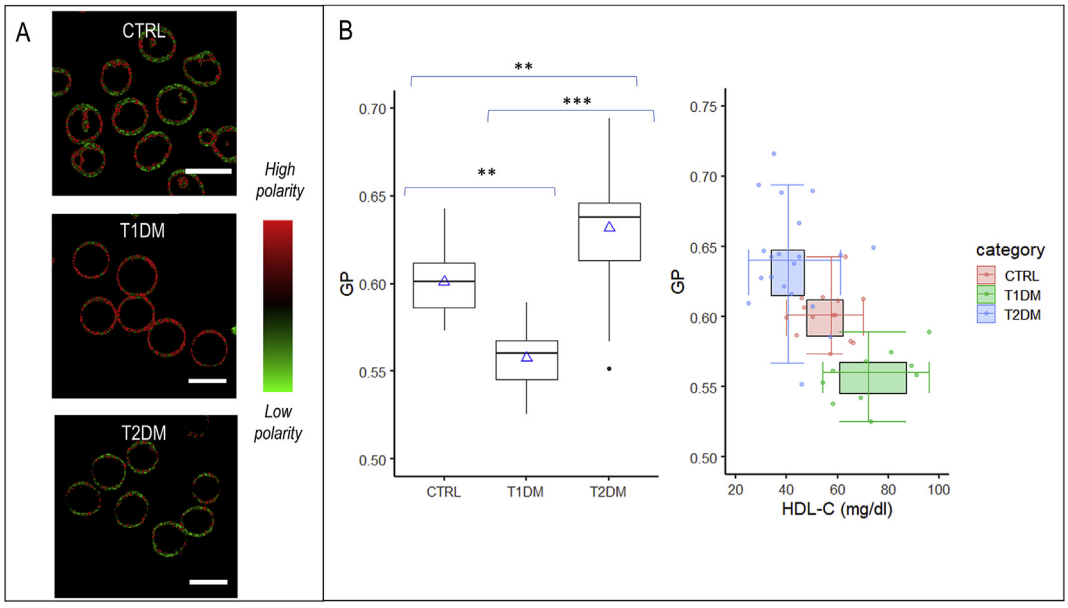

Fig. 3. Micropolarity maps of healthy, T1DM and T2DM RBC (A) Submicrometric phase state map of healthy, T1DM and T2DM RBC are reported. Each pixel is colored according to its GP values, in a two-colored scale spanning from red (high polarity, low GP) to green (low polarity high GP). (B) The box plot shows significant differences among the GP values of the three populations under observation (** stands for p <0.01; *** stands for p<0.001). The double box plot shows GP average values in each group plotted versus HDL average values. (For interpretation of the references to color in this figure legend, the reader is referred to the Web version of this article.)

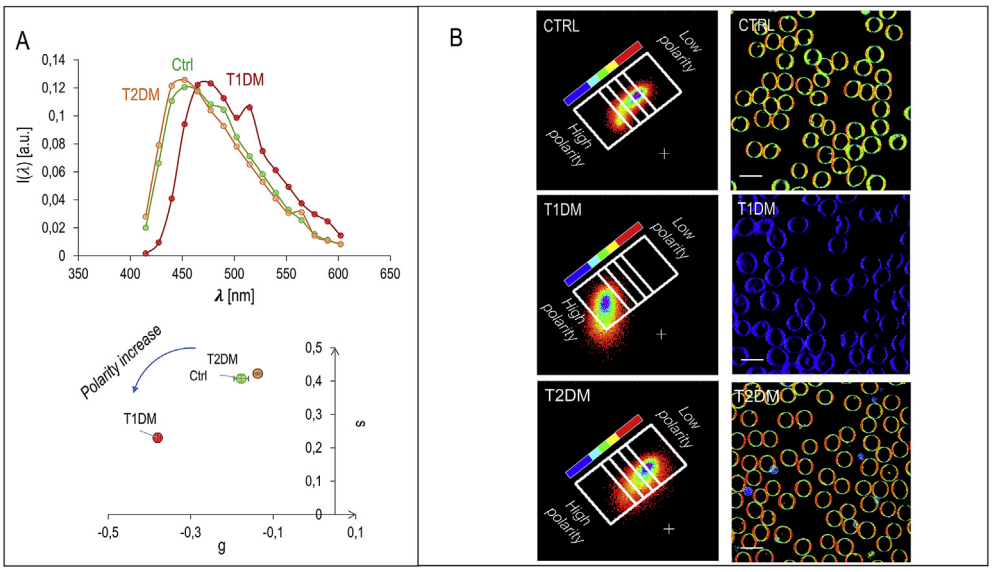

Fig. 4. Spectral analysis of laurdan emission of healthy, T1DM and T2DM RBC (A) spectra of laurdan in healthy, T1DM and T2DM RBC. The already observed increase in environmental membrane micropolarity (GP decrease), is detectable by the shift in the red-shifted emission. (B) Spectral phasor analysis method. The pixels selected in the blue ROI corresponds to the regions with the lowest membrane micropolarity, while the pixels in the red ROI corresponds to the highest membrane micropolarity. Regions characterized by an intermediate micropolarity value are shown in a pseudo-colored scale from red to blue (figure lookup table along with the phasor plot). The color-coded regions of interest are chosen as rectangles, with the shortest sides perpendicular to the line connecting the center of mass of the clouds in the phasor plot of untreated and treated cells. (For interpretation of the references to color in this figure legend, the reader is referred to the Web version of this article.)

In Fig. 4A the spectra of laurdan in healthy, T1DM and T2DM RBC are reported. The already observed increase in environmental membrane micropolarity (GP decrease), is detectable by the shift in the emission wavelength towards the green. As done with the cholesterol depletion experiment, laurdan fluorescence emission spectrum, registered with pixel resolution, can be further analyzed by the spectral phasor analysis method [19,23,24]. In Fig. 4B, pixels selected in the blue ROI corresponds to the regions with the lowest membrane micropolarity, while the pixels in the red ROI corresponds to the highest membrane micropolarity. Regions characterized by an intermediate micropolarity value are shown in a pseudo-colored scale from red to blue (figure look-up table along with the phasor plot in Fig. 4B). The color-coded regions of interest are chosen as rectangles, with the shortest sides perpendicular to the line connecting the center of mass of the clouds in the phasor plot of untreated and treated cells. From the phasor-segmented images, it is again evident the presence of highly packed regions in T2DM patients. These regions decrease in number in CTRL and are almost absent in T1DM. Again, the low-polarity regions are organized in domains characterized by a high-packing density. The opposite trend in both quantities can conversely be observed in T2DM RBC.

3.4. Membrane microviscosity of RBC from healthy subjects and T1DM and T2DM patients

To investigate the viscosity effects, we analyze the green channel decay time in the three groups (Fig. 5A). With respect to control, T1DM RBC present a decrease of the apparent lifetime of the green channel indicating a less viscous environment and a decrease of the lifetime of the relaxed state indicating a more polar environment. On the contrary, T2DM RBC present an augmented contribution of the non-exponential decay in control cells. To dissect these two contributions we can use the lifetime phasor transformation (section 3.2). The phasor distribution integrated for N = 90 cells (in each category) shows the center of mass of the phasor that lies outside of the universal circle for the control cells, indicating a non-exponential decay. In T1DM patients, the point rotates towards the universal circle. T2DM RBC are characterized by a non-exponential decay indicating a more viscous environment with respect to control cells. We select regions in the phasor plot and remap them to the original fluorescence images, thus providing a viscosity driven segmentation: pixels characterized by a similar viscosity value can be grouped and shown on the image with a characteristic color scale. The color-coded regions of interest are chosen as rectangles, with the shortest sides perpendicular to the line connecting the center of mass of the clouds in the phasor plot of untreated and treated cells. From the lifetime images it is possible to observe that high lipid packing domains, characterized by low polarity, display also high viscosity, and they progressively disappear in going from T2DM, through CTRL to T1DM.

4. Discussion

In this article we proposed RBC membrane micropolarity as a diagnostic classifier for distinguish between the two main types of diabetes. We have found a less polar, more viscous membrane microenvironment organized in sub-micrometric domains in T2DM patients, and a more polar, less viscous membrane microenvironment in T1DM patients and in cholesterol depletion experiment compared to control healthy patients.

We have observed how cholesterol has a role in the variation in micropolarity and microviscosity. Membrane micropolarity values depend on lipid structure, packing, and composition, and increases with membrane hydration levels [25,26]. We have shown how the short cholesterol molecules alter the phase state of the RBC membrane, by filling these spaces between neighboring phospholipids, making the plasma membrane less flexible, as well as less permeable, thus effectively dewetting the intermembrane spaces [29]. At a molecular level, experimental results show that there are about five tightly hydrogen-bonded water molecules with the oxygen atoms per phospholipid molecule in PC [30,31], and cholesterol affects these interactions [4–6]. The cholesterol hydroxyl group can act both as hydrogen bond donor and acceptor, and can

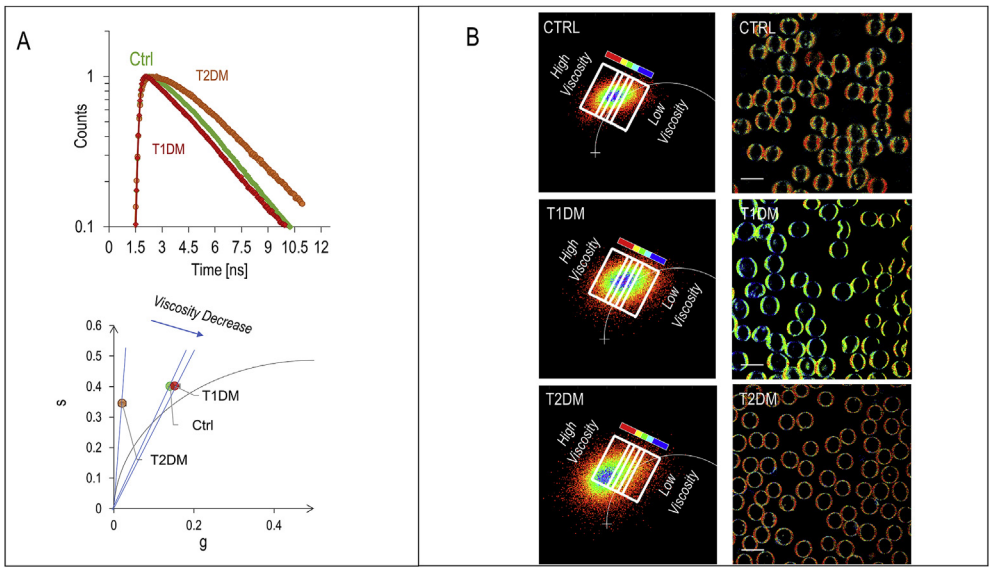

Fig. 5. Lifetime analysis of laurdan emission of healthy, T1DM and T2DM RBC (A) decay curves in the green channel emission(540/50 nm) for healthy, T1DM and T2DM RBC. The corresponding Lifetime phasor transformation allows us to quantify and visualize changes in viscosity. The phasor distribution integrated for N = 90 cells (in each category) shows the center of mass of the phasor that lies outside of the universal circle for the control cells, indicating a non-exponential decay. In T1DM patients, the point rotates towards the universal circle, while T2DM RBC moves away from the universal circle. This shift indicates a more viscous environment with respect to control cells. (B)Viscosity driven segmentations of RBC cells. Segmentations are colored from blue (low viscosity) to red (high viscosity). Figure lookup table is reported along with the phasor plot. The color-coded regions of interest are chosen as rectangles, with the shortest sides perpendicular to the line connecting the center of mass of the clouds in the phasor plot of untreated and treated cells. (For interpretation of the references to color in this figure legend, the reader is referred to the Web version of this article.)

also participate in charge pairing. That gives cholesterol the versatility to form numerous different types of bonds in the interfacial region. In molecular dynamics (MD) and NMR studies on model membranes of DPPC [5] and DMPC [32,33], it is shown that cholesterol prefers interactions with DPPC rather than water. The overall decrease of the extent of hydrogen-bonded water molecules with phospholipids ultimately explains the decrease in micropolarity we have observed in fluorescence lifetime measurements.

Along with micropolarity, we have analyzed membrane microviscosity, which depends on the rotational diffusional processes, and it is strongly linked to the water-membrane interaction extent. The reduction of microviscosity upon cholesterol depletion can be also ascribed to cholesterol, affecting the interactions of water molecules at the bilayer interface [4–6] Indeed it is shown in in MD experiments on model membranes [34,35,36,37] that cholesterol is capable of forming “water bridges” [6], which are indirect, water-mediated lipid–lipid interactions. These interactions can form H-bond networks at the membrane interface [37], which can help to stabilize the membrane structure similar to structural water in proteins [36]. The lifetime of these water bridges is of the order of 500 ps [4], which is an order of magnitude higher than the lifetime of cholesterol-carbonyl oxygen in the DMPC-Chol bilayer (70 ps), or to that of cholesterol-water (~40 ps) [4]. According to these observations, the increase in microviscosity observed in presence of cholesterol can be due to the formation of water bridges, whose interaction lifetime is in agreement with the observed delay in the fluorescence lifetime of the excited state of laurdan which lasts for ~1000 ps (see the first exponential decay in Fig. 5A). Conversely, the estimated lifetime increase due to Chol-water/Cholesterol phospholipid interaction would be too small to be revealed with our experimental setup.

Based on these observations, we hypothesize that micropolarity and microviscosity are affected by the pathologic alterations of cholesterol homeostasis occurring in T1DM and T2DM. RBCs, devoid of lipoprotein receptors, exchange cholesterol and phospholipid exclusively by the free diffusion pathway [38]. Cholesterol exchanges freely between RBC, plasma, circulating lipoproteins, and cells [39]. Moreover, RBC may participate in the transport of cholesterol from tissues to the liver [40]. Approximately 50% of circulating cholesterol is carried in RBC membranes and tracer studies in humans indicate that the magnitude of the cholesterol flux through RBC is comparable to the total efflux of free cholesterol from tissues [41]. The steady-state level of cholesterol available for free exchange, therefore, alter the physical state of blood cell membranes, varying the hydration and the structure of bound water layer. A further indication of the role of cholesterol efflux can be found in the negative correlation of micropolarity with HDL-C content (Fig. 3B): the free cholesterol efflux from cells to HDL in the extracellular medium is promoted by metabolic trapping in which the return of released cholesterol to the cell is prevented by esterification when lecithin-cholesterol acyltransferase acts on HDL [42].

In this view, the steady-state level of cholesterol available for free exchange with RBC is altered and thus sensed at a different extent in T1DM and T2DM: patients with diabetes present lipid disorders, which are in general distinct for the T1DM, resulting from the pancreas’ failure to produce enough insulin, and T2DM, which begins with insulin resistance, a condition in which cells fail to respond to insulin properly [43]. Specifically, several qualitative abnormalities of lipoproteins, which are potentially atherogenic, are observed in patients with T1DM, even in those with good metabolic control. These abnormalities include increased cholesterol-to-triglyceride ratios within very low-density Lipoproteins (VLDL), increased triglycerides in LDL and HDL, compositional changes in the peripheral layer of lipoproteins, glycation of apolipoproteins, increased oxidation of LDL and an increase in small, dense LDL particles [44,45]. On the contrary, patients with T2DM could have dyslipidemia at varying degrees, characterized by increased levels of triglycerides and decreased serum HDL-C [45,46]. It should, however, be noted that the classification efficiency of the assay may be ascribed to other factors than cholesterol: in principle, also phospholipid transfer between lipoproteins

and RBC may play a role in altering the water structure at the membrane-water interface. However, the halftime of free transfer of cholesterol at 37 °C is ~2h, while the one of dipalmitoylphosphocoline (DPPC) is ~83 h. The fact that the rate of transfer of this phospholipid is 2.5% with respect of cholesterol furnishes an indication that, among the transferred lipids, cholesterol can be a major determinant in the observed variations [47,48]. As already pointed out in Ref. [10], in this diagnostic system, the *output* is the variation in micropolarity, and the biophysical process connecting input and output consists in a network of systemic effects related to the chronic hyperglycemia, oxidative stress and metabolic alterations triggered by the systemic state (glyco-oxidation), rather than the glycosylation of a single protein (as in the traditional HbA1C assay). These conditions are a source of permanent, cumulative damage to RBC membranes in diabetes, integrated over an average period of three months. Indeed, RBC are uniquely vulnerable to these effects, due to their inability to synthesize new proteins and degrade altered, non-functional proteins. Glycosylation and oxidation, expression of the systemic state, and therapy-dependent membrane remodeling lead, throughout the outlined integrated network, to RBC micropolarity variation in different ways for T1DM and T2DM. The significant differences among the selected groups can be explained by the potential of membrane polarity of RBC to integrate the different systemic effects of T1DM and T2DM on blood serum. Single, more specific blood values, representing only the presence of a particular protein or metabolite, cannot discriminate by themselves with enough significance among the different diseases. The main limit of this work is the small sample size, and the validation of the approach on a larger population is necessary. However, this investigation paves the possibility for the use of the RBC micropolarity assay in diagnostics, in assessing the response to therapies and in fully describing the progression of T1DM and T2DM, complementing HbA1c in defining the quality of long-term management of diabetes [10,49].

Author contributions

Conceptualization, GM.; Methodology, GM, FD, GB, DP; Software, GM, FD; Validation, GM, GB, DP, GER.; Formal Analysis, GB, GM, GC,AR, FD, GER.; Investigation, GM, GB, FD, GER, AF, ED, MD.; Resources, GM, GC, AR, AF, FD, GER, ED, MD.; Data Curation, GB, FD, GER, ED, MD, GC, AR; Writing-Original Draft Preparation, GM.; Writing-Review & Editing, GM,GB, DP, FD,MD; Visualization, GB, FD, GER, ED, MD; Supervision, GM; Project Administration, GM,DP,MD; Funding Acquisition, GM.

Declaration of competing interest

The authors declare that they have no known competing financial interests or personal relationships that could have appeared to influence the work reported in this paper.

Acknowledgments

The authors acknowledge Mario Amici for his excellent Technical support. All authors have read the journal's authorship agreement and policy on disclosure of potential conflicts of interest. This work was supported by Università Cattolica del Sacro Cuore Linea D1 2015 grant number R4124500312 and funded through an EFSD award, supported by EFSD and Sanofi European Pilot Research Grants for Innovative Measurement of Diabetes Outcomes."

Appendix A. Supplementary data

Supplementary data to this article can be found online at https://doi.org/10.1016/j.acax.2019.100030.

References

[1] A.D. American Diabetes Association, Diagnosis and classification of diabetes mellitus, Diabetes Care 32 (Suppl 1) (2009) S62–S67, https://doi.org/10.2337/dc09-S062.
[2] R.P. Rand, V.A. Parsegian, Hydration forces between phospholipid bilayers, Biochim. Biophys. Acta Rev. Biomembr. 988 (1989) 351–376, https://doi.org/10.1016/0304-4157(89)90010-5.
[3] R. Reinhard Lipowsky, E. Erich Sackmann, Structure and Dynamics of Membranes, Elsevier Science, 1995. https://www.sciencedirect.com/handbook/handbook-of-biological-physics/vol/1/suppl/C. (Accessed 2 May 2019).
[4] M. Pasenkiewicz-Gierula, T. Róg, K. Kitamura, A. Kusumi, Cholesterol effects on the phosphatidylcholine bilayer polar region: a molecular simulation study, Biophys. J. 78 (2000) 1376–1389, https://doi.org/10.1016/S0006-3495(00)76691-4.
[5] T. Róg, M. Pasenkiewicz-Gierula, I. Vattulainen, M. Karttunen, What happens if cholesterol is made smoother: importance of methyl substituents in cholesterol ring structure on phosphatidylcholine–sterol interaction, Biophys. J. 92 (2007) 3346–3357, https://doi.org/10.1529/BIOPHYSJ.106.095497.
[6] T. Róg, M. Pasenkiewicz-Gierula, I. Vattulainen, M. Karttunen, Ordering effects of cholesterol and its analogues, Biochim. Biophys. Acta Biomembr. 1788 (2009) 97–121, https://doi.org/10.1016/J.BBAMEM.2008.08.022.
[7] D. Wüstner, K. Solanko, How cholesterol interacts with proteins and lipids during its intracellular transport, Biochim. Biophys. Acta Biomembr. 1848 (2015) 1908–1926, https://doi.org/10.1016/J.BBAMEM.2015.05.010.
[8] D.P. Mikhailidis, M. Elisaf, M. Rizzo, K. Berneis, B. Griffin, A. Zambon, V. Athyros, J. de Graaf, W. März, K.G. Parhofer, G.B. Rini, G.A. Spinas, G.H. Tomkin, A.D. Tselepis, A.S. Wierzbicki, K. Winkler, M. Florentin, E. Liberopoulos, European panel on low density lipoprotein (LDL) subclasses": a statement on the pathophysiology, atherogenicity and clinical significance of LDL subclasses. Curr. Vasc. Pharmacol. 9 (2011) (February 8, 2019), 533–71, http://www.ncbi.nlm.nih.gov/pubmed/21595628.
[9] C. Constantinou, E.A. Karavia, E. Xepapadaki, P.-I. Petropoulou, E. Papakosta, M. Karavyraki, E. Zvintzou, V. Theodoropoulos, S. Filou, A. Hatziri, C. Kalogeropoulou, G. Panayiotakopoulos, K.E. Kypreos, Advances in high-density lipoprotein physiology: surprises, overturns, and promises, Am. J. Physiol. Metab. 310 (2016) E1–E14, https://doi.org/10.1152/ajpendo.00429.2015.
[10] G. Maulucci, E. Cordelli, A. Rizzi, F. De Leva, M. Papi, G. Ciasca, D. Samengo, G. Pani, D. Pitocco, P. Soda, G. Ghirlanda, G. Iannello, M. De Spirito, Phase separation of the plasma membrane in human red blood cells as a potential tool for diagnosis and progression monitoring of type 1 diabetes mellitus, PLoS One 12 (2017), e0184109, https://doi.org/10.1371/journal.pone.0184109.
[11] R.B. Macgregor, G. Weber, Fluorophores in polar media: spectral effects of the Langevin distribution of electrostatic InteractionS, Ann. N. Y. Acad. Sci. 366 (1981) 140–154, https://doi.org/10.1111/j.1749-6632.1981.tb20751.x.
[12] G. Maulucci, D. Troiani, S.L.M. Eramo, F. Paciello, M.V. Podda, G. Paludetti, M. Papi, A. Maiorana, V. Palmieri, M. De Spirito, A.R. Fetoni, Time evolution of noise induced oxidation in outer hair cells: role of NAD(P)H and plasma membrane fluidity, Biochim. Biophys. Acta Gen. Subj. 1840 (2014), https://doi.org/10.1016/j.bbagen.2014.04.005.
[13] J.R. Lakowicz, Principles of Fluorescence Spectroscopy, Springer, 2006.
[14] L.A. Bagatolli, E. Gratton, Two photon fluorescence microscopy of coexisting lipid domains in giant unilamellar vesicles of binary phospholipid mixtures, Biophys. J. 78 (2000) 290–305, https://doi.org/10.1016/S0006-3495(00)76592-1.
[16] G. Weber, F.J. Farris, Synthesis and spectral properties of a hydrophobic fluorescent probe: 6-propionyl-2-(dimethylamino)naphthalene, Biochemistry 18 (1979) 3075–3078, https://doi.org/10.1021/bi00581a025.
[17] G. Maulucci, O. Cohen, B. Daniel, A. Sansone, P.I. Petropoulou, S. Filou, A. Spyridonidis, G. Pani, M. De Spirito, C. Chatgilialoglu, C. Ferreri, K.E. Kypreos, S. Sasson, Fatty acid-related modulations of membranes fluidity in cells: detection and implications, Free Radic. Res. 0 (2016) 1–22, https://doi.org/10.1080/10715762.2016.1231403.
[18] G. Maulucci, M. Chiarpotto, M. Papi, D. Samengo, G. Pani, M. De Spirito, Quantitative analysis of autophagic flux by confocal pH-imaging of autophagic intermediates, Autophagy 11 (2015) 1905–1916, https://doi.org/10.1080/15548627.2015.1084455.
[19] G. Maulucci, F. Di Giacinto, C. De Angelis, O. Cohen, B. Daniel, C. Ferreri, M. De Spirito, S. Sasson, Real time quantitative analysis of lipid storage and lipolysis pathways by confocal spectral imaging of intracellular micropolarity, Biochim. Biophys. Acta Mol. Cell Biol. Lipids 1863 (2018) 783–793, https://doi.org/10.1016/J.BBALIP.2018.04.004.
[20] F. Fereidouni, A.N. Bader, H.C. Gerritsen, Spectral phasor analysis allows rapid and reliable unmixing of fluorescence microscopy spectral images, Opt. Express 20 (2012) 12729–12741.
[21] M.A. Digman, V.R. Caiolfa, M. Zamai, E. Gratton, The phasor approach to fluorescence lifetime imaging analysis, Biophys. J. 94 (2008) L14–L16, https://doi.org/10.1529/biophysj.107.120154.
[22] F. Di Giacinto, C. De Angelis, M. De Spirito, G. Maulucci, Quantitative imaging of membrane micropolarity in living cells and tissues by spectral phasors

analysis, Methods 5 (2018) 1399–1412, https://doi.org/10.1016/j.mex.2018.10.010.
[23] F. Fereidouni, A.N. Bader, A. Colonna, H.C. Gerritsen, Phasor analysis of multiphoton spectral images distinguishes autofluorescence components of in vivo human skin, J. Biophot. (2013), https://doi.org/10.1002/jbio.201200244.
[24] L. Malacrida, D.M. Jameson, E. Gratton, A multidimensional phasor approach reveals LAURDAN photophysics in NIH-3T3 cell membranes, Sci. Rep. 7 (2017) 9215, https://doi.org/10.1038/s41598-017-08564-z.
[25] P. Jurkiewicz, J. Sýkora, A. Olżyńska, J. Humpolíčková, M. Hof, Solvent relaxation in phospholipid bilayers: principles and recent applications, J. Fluoresc. 15 (2005) 883–894, https://doi.org/10.1007/s10895-005-0013-4.
[26] P. Jurkiewicz, A. Olżyńska, M. Langner, M. Hof, Headgroup hydration and mobility of DOTAP/DOPC bilayers: a fluorescence solvent relaxation study, Langmuir 22 (2006) 8741–8749, https://doi.org/10.1021/la061597k.
[27] O. Golfetto, E. Hinde, E. Gratton, Laurdan fluorescence lifetime discriminates cholesterol content from changes in fluidity in living cell membranes, Biophys. J. 104 (2013) 1238–1247, https://doi.org/10.1016/j.bpj.2012.12.057.
[28] Y. Ma, A. Benda, J. Kwiatek, D.M. Owen, K. Gaus, Time-resolved laurdan fluorescence reveals insights into membrane viscosity and hydration levels, Biophys. J. 115 (2018) 1498–1508, https://doi.org/10.1016/J.BPJ.2018.08.041.
[29] R.A. Cooper, Influence of increased membrane cholesterol on membrane fluidity and cell function in human red blood cells, J. Supramol. Struct. 8 (1978) 413–430, https://doi.org/10.1002/jss.400080404.
[30] K. Arnold, L. Pratsch, K. Gawrisch, Effect of poly(ethylene glycol) on phospholipid hydration and polarity of the external phase, Biochim. Biophys. Acta 728 (1983) 121–128. http://www.ncbi.nlm.nih.gov/pubmed/6687553. accessed May 2, 2019.
[31] S. König, E. Sackmann, D. Richter, R. Zorn, C. Carlile, T.M. Bayerl, Molecular dynamics of water in oriented DPPC multilayers studied by quasielastic neutron scattering and deuterium-nuclear magnetic resonance relaxation, J. Chem. Phys. 100 (1994) 3307–3316, https://doi.org/10.1063/1.466422.
[32] M. Pasenkiewicz-Gierula, T. Róg, K. Kitamura, A. Kusumi, Cholesterol effects on the phosphatidylcholine bilayer polar region: a molecular simulation study, Biophys. J. 78 (2000) 1376–1389, https://doi.org/10.1016/S0006-3495(00)76691-4.
[33] O. Soubias, F. Jolibois, A. Milon, V. Réat, High-resolution 13C NMR of sterols in model membrane, Compt. Rendus Chem. 9 (2006) 393–400, https://doi.org/10.1016/j.crci.2005.06.015.
[34] T. Róg, K. Murzyn, M. Pasenkiewicz-Gierula, The dynamics of water at the phospholipid bilayer surface: a molecular dynamics simulation study, Chem. Phys. Lett. 352 (2002) 323–327, https://doi.org/10.1016/S0009-2614(02)00002-7.
[35] T. Róg, M. Pasenkiewicz-Gierula, Cholesterol effects on a mixed-chain phosphatidylcholine bilayer: a molecular dynamics simulation study, Biochimie 88 (2006) 449–460, https://doi.org/10.1016/j.biochi.2005.10.005.
[36] M. Pasenkiewicz-Gierula, Y. Takaoka, H. Miyagawa, K. Kitamura, A. Kusumi, Hydrogen bonding of water to phosphatidylcholine in the membrane as studied by a molecular dynamics simulation: location, geometry, and Lipid–Lipid bridging via hydrogen-bonded water, J. Phys. Chem. A 101 (1997) 3677–3691, https://doi.org/10.1021/jp962099v.
[37] M. Pasenkiewicz-Gierula, Y. Takaoka, H. Miyagawa, K. Kitamura, A. Kusumi, Charge pairing of headgroups in phosphatidylcholine membranes: a molecular dynamics simulation study, Biophys. J. 76 (1999) 1228–1240, https://doi.org/10.1016/S0006-3495(99)77286-3.
[38] G.J. Nelson, Composition of neutral lipids from erythrocytes of common mammals, J. Lipid Res. 8 (1967) 374–379. http://www.ncbi.nlm.nih.gov/pubmed/6033604.
[39] J.S. HAGERMAN, R.G. GOULD, The in vitro interchange of cholesterol between plasma and red cells, in: Proc. Soc. Exp. Biol. Med., vol. 78, 1951, pp. 329–332. http://www.ncbi.nlm.nih.gov/pubmed/14892010. accessed September 4, 2018.
[40] J.A. Glomset, The plasma lecithins:cholesterol acyltransferase reaction, J. Lipid Res. 9 (1968) 155–167. http://www.ncbi.nlm.nih.gov/pubmed/4868699. accessed September 4, 2018.
[41] S. Turner, J. Voogt, M. Davidson, A. Glass, S. Killion, J. Decaris, H. Mohammed, K. Minehira, D. Boban, E. Murphy, J. Luchoomun, M. Awada, R. Neese, M. Hellerstein, Measurement of reverse cholesterol transport pathways in humans: in vivo rates of free cholesterol efflux, esterification, and excretion, J. Am. Heart Assoc. 1 (2012), e001826, https://doi.org/10.1161/JAHA.112.001826.
[42] H. Czarnecka, S. Yokoyama, Regulation of cellular cholesterol efflux by lecithin:cholesterol acyltransferase reaction through nonspecific lipid exchange, J. Biol. Chem. 271 (1996) 2023–2028, https://doi.org/10.1074/JBC.271.4.2023.
[43] S. Chatterjee, K. Khunti, M.J. Davies, Type 2 diabetes, Lancet 389 (2017) 2239–2251, https://doi.org/10.1016/S0140-6736(17)30058-2.
[44] B. Vergès, Lipid disorders in type 1 diabetes, Diabetes Metab. 35 (2009) 353–360, https://doi.org/10.1016/j.diabet.2009.04.004.
[45] A.A. Rivellese, O. Vaccaro, L. Patti, The pathophysiology of lipid metabolism and diabetes, Int. J. Clin. Pract. 58 (2004) 32–35, https://doi.org/10.1111/j.1368-504X.2004.00332.x.
[46] A.D. Mooradian, Dyslipidemia in type 2 diabetes mellitus, Nat. Rev. Endocrinol. 5 (2009) 150–159, https://doi.org/10.1038/ncpendmet1066.
[47] D.B. Zilversmit, M.E. Hughes, Phospholipid exchange between membranes, in: Methods Membr. Biol., Springer US, Boston, MA, 1976, pp. 211–259, https://doi.org/10.1007/978-1-4757-5820-7_4.
[48] M.C. Phillips, Molecular mechanisms of cellular cholesterol efflux, J. Biol. Chem. 289 (2014) 24020–24029, https://doi.org/10.1074/jbc.R114.583658.
[49] E. Cordelli, G. Maulucci, M. De Spirito, A. Rizzi, D. Pitocco, P. Soda, A decision support system for type 1 diabetes mellitus diagnostics based on dual channel analysis of red blood cell membrane fluidity, Comput. Methods Progr. Biomed. 162 (2018), https://doi.org/10.1016/j.cmpb.2018.05.025.